PCCP

Accepted Manuscript

ROYAL SOCIETY OF CHEMISTRY

www.rsc.org/pccp

Self-generated concentration and modulus gradients coating design to protect Si nano-wire electrodes during lithiation

Sung-Yup Kim[a], Alireza Ostadhossein[b], Adri C.T. van Duin[b], Xingcheng Xiao[c], Huajian Gao[d], and Yue Qi[a,*]

[a]Department of Chemical engineering & Material Science, Michigan State University, East Lansing, MI48824, USA
[b]Department of Mechanical & Nuclear Engineering, Pennsylvania State University, University Park, PA16802, USA
[c]General Motors Global Research & Development Center, 30500 Mound Road, Warren, MI 48090, USA
[d]School of Engineering, Brown University, Providence, RI 02912, USA

ABSTRACT

Surface coatings as artificial solid electrolyte interphase have been actively pursued as an effective way to improve the cycle efficiency of nanostructured Si electrodes for high energy density lithium ion batteries, where the mechanical stability of the surface coatings on Si is as critical as Si itself. However, the chemical composition and mechanical properties change of coating materials during lithiation and delithiation process imposed a grand challenge to design coating/Si nanostructure as an integrated electrode system. In our work, we first developed reactive force field (ReaxFF) parameters for Li-Si-Al-O materials to simulate the lithiation process of Si-core/Al_2O_3-shell and Si-core/SiO_2-shell nanostructures. With reactive dynamics simulation, we were able to simultaneously track and correlate the lithiation rate, compositional change, mechanical property evolution, stress distributions, and fracture. A new mechanics model based on these varying properties was developed to determine how to stabilize the coating with a critical size ratio. Furthermore, we discovered that the self-accelerating Li diffusion in Al_2O_3 coating forms a well-defined Li concentration gradient, leading to an elastic modulus gradient, which effectively avoids local stress concentration and mitigates crack propagation. Based on these results, we propose a modulus gradient coating, softer outside, harder inside, is the most efficient coating to protect Si electrode surface and improve its current efficiency.

*Corresponding Author**:** yueqi@egr.msu.edu, 5174321243

1. Introduction

Silicon (Si) has long been considered as a promising high capacity negative electrode in lithium ion batteries [1-4] to meet the demand from portable energy storage devices to large-scale transportation applications. However, the use of high capacity Si based negative electrode has been limited by its mechanical degradation caused by the large volume expansion/contraction during cycling [5,6]. Nanostructured Si [2, 3, 7-9], especially below some critical sizes [10, 11], can mitigate Si fracture [3, 11], thus becoming a promising solution. However, the high surface to volume ratio of nanostructures along with the large volume change of Si, lead to unacceptable amount of solid-electrolyte interphase (SEI) formation [12] and growth [13, 14], which causes low current/columbic efficiency and short life [15, 16]. To address the problem, multi-functional coatings, such as carbon [17-19], Cu [20], Al [21], Al_2O_3 [22-25], TiO_2 [9, 26], TiN [26], SiO_2 and carbon double shells [27], have been developed as possible artificial SEI layers to improve the performance and life of silicon electrode. Among these artificial SEI coatings, atomic layer deposited (ALD) coatings [22-25] have been shown to slow down or reduce SEI formation by changing the reduction process of ethylene carbonate (EC) electrolyte solvent [28-32]. In fact, even the 2~5 nm thick native oxide layer on Si NWs can reduce the side reactions during the first lithiation cycle [7, 15]. This is likely due to the electronic insulating and high dielectric properties of Al_2O_3 and SiO_2 [33].

Due to the multi-functions of the coatings, their electronic and ionic conductivity, mechanical strength, and geometry will jointly alter the lithiation rates, lithium concentration gradient in Si, and consequently mitigate the diffusion-induced-stress and crack generation [34-36]. When a long Si nanowire is lithiated under *in situ* transmission electron microscopy (TEM) from one end,

electronic conductive coatings, such as carbon [17-19] and Cu [20] can speed up the lithiation rate of the Si nanowires along the axial direction significantly, and even alter the shape of crystalline Si nanowire. Sandu et al.[37] used crystalline-Si-core/nickel-shell nanopillars as a model system to investigate the effect of coating thickness to pillar diameter ratio on fracture patterns. Thicker coatings changed the anisotropic lithiation of *c*-Si NW [38] into an isotropic process and caused less cracking. However, electrodes made of Si nano-arrays or nano-particles will be lithiated along the radial direction rather than the axial direction, so the electronic conductive coating, such as TiN did not show much advantage [26]. Instead, conformal Li activated oxide coatings, such as TiO_2 [9, 26] on Si NW, demonstrated a dramatic performance improvement in terms of coulombic efficiency and capacity retention. Memarzadeh *et al.* [21] also showed that co-lithiation of an Al shell on the Si nanowire creates a compressive stress on the Si core and effectively reduced the magnitude of their cracking/disintegration. Typical SEI formed by electrolyte reduction reactions contains Li_2CO_3 and LiF and some organic components, which will not be further lithiated during cycling. On the other hand, many coating materials, such as SiO_2, Al_2O_3, TiO_2, and Al, do change their chemistry and properties during battery operation.[9, 22-27] Theoretically, artificial SEI coating can be mechanically stable to withstand the volume change in Si during lithiation and delithiation, if the material properties, thickness of the coating, and the size/shape of Si can be optimized. However, the search for optimized coating materials and thickness is complicated by the chemical evolution of the coatings, as it will lead to volume and property changes. In order to understand the impact of coating lithiation on its mechanical stability, we will compare the lithiation process of Si core-shell structures with amorphous SiO_2 and Al_2O_3 shells via atomic simulations. Such comparison will be important to many experimental studies trying to compare the ALD-Al_2O_3 coated Si with

uncoated Si, while the uncoated Si is typically terminated by a few-nanometer-thick native SiO_2[39] layer.

Both Al_2O_3 and SiO_2 coatings have shown improved performance due to the combined effect of passivating the Si surface, constraining Si deformation, and reducing cracks [7, 22-24, 40, 41]. While thicker coating can mitigate cracking of Si more effectively, it may block Li ion transport, thus an optimized coating thickness needs to be obtained. Xiao et al.[40] observed that a ~ 5nm thick Al_2O_3 coated 75nm thick Si thin film showed much fewer cracks than the uncoated Si film. Nguyen et al.[24] observed a 9nm thick Al_2O_3 layer coated on Si-based nanowire arrays (~50nm thick a-Si on 75nm diameter of NiSi core) cracked but still protected the Si and extended the cycle life compared to non-coated samples. McDowell et al.[7] suggested that a native SiO_2 layer with a thickness of 2~5 nm can suppress the volume expansion of Si nanowires with diameters less than ~50nm. This is partially due to oxide-induced compressive stress could shift the chemical potential of Li and limit the amount of lithiation of the Si (at the same open circuit voltage but stress free) [42, 43]. Artificial SiO_2 coatings with thickness ranging from 2~15 nm were compared by Sim et. al. [41] and the 7nm thick coating was identified as optimal in suppressing volume expansion of Si while still allowing fast Li diffusion.

To fully understand the benefits of SiO_2 and Al_2O_3 coating on Si, the evolution of the chemical composition, diffusion and mechanical properties of the coatings during cycling must be taken into account. Philippe et al.[44] showed that reaction of SiO_2 with lithium after cycling leads to an increase of Li_4SiO_4 which has long been shown as Li ionic conductor [45, 46]. This is not surprising as SiO_x can be an anode material itself [47]. Xiao et al.[40] found that the structure of the Al_2O_3 coating changes to $Al_2O_3/AlF_3/LiAlO_2$ after cycling. Wang et al.[48] stated that the co-existence of AlF_3 and Al_2O_3 is beneficial for improving the ionic conductivity in the SEI layer.

The initial Li diffusion barrier in Al_2O_3 is extremely high, as predicted by density functional theory (DFT) calculations [49, 50]. The lithiation of Al_2O_3 into $LiAlO_2$ on the top surface has been proven to reduce the diffusion energy barrier of Li diffusion [49-51]. Kim and Qi [49] performed DFT calculations to investigated the property evolution of Al_2O_3 and SiO_2 upon lithiation and found that the Young's modulus and Li diffusion energy barrier in Al_2O_3 decrease significantly upon lithiation. The naturally formed 4-5nm thick Al_2O_3 layer covering aluminum nanowires was also demonstrated to form a stretchable and stable Li-Al-O amorphous layer under *in situ* TEM [25].

The role of the chemical evolution of the coating materials on the lithiation kinetics, mechanical deformation of the Si electrode and the failure mechanism of the coating itself are rarely discussed, partly due to the fact that it is difficult to simultaneously track the chemical, structural, and mechanical evolution of the nano-structures experimentally and computationally. In this paper, we tracked these changes during lithiation of Si core-shell structures at atomic scale, with reactive molecular dynamics (MD) and a newly developed reactive force field (ReaxFF) for Li-Al-Si-O system. This ReaxFF is built upon the Li-Si-O system [52, 53], which has been used to illustrate compressive stress caused by the SiO_2 coating can slow down the lithiation process [54] via MD simulations. In this study, amorphous Al_2O_3 and SiO_2 covered Si nanowires were compared. The amorphous SiO_2 represents naturally formed oxides on Si nanowire and Al_2O_3 represents an ALD-Al_2O_3 coating on Si nanowires. The details of lithiation mode, fracture mechanism, and stress distribution of the ALD coating during lithiation of the Si-core-shell structure were analyzed. To our surprise, we found that the increasing Li diffusion in Li-Al-O system with increasing Li content leads to a well-defined Li density gradient along the coating thickness. This Li density gradient leads to an elastic modulus gradient (harder inside

and softer outside) and plays a critical role in avoiding local stress concentration and crack generation. This natural gradient coating provides a new avenue for coating design on nano-structured Si electrodes.

2. Computational Methods

In the ReaxFF method, the energies and forces are derived from a general energy expression

$$E_{system} = E_{bond} + E_{over} + E_{under} + E_{lp} + E_{val} + E_{vdWaals} + E_{coulomb} \quad (1)$$

The partial contributions in Eq. (1) include bond energies (E_{bond}), energy to penalize over-coordination (E_{over}) and stabilize under-coordination of atoms (E_{under}), lone-pair energies (E_{lp}), valence angle energies (E_{val}) and terms to handle non-bonded Coulomb ($E_{coulomb}$) and van der Waals ($E_{vdWaals}$) interaction energies. All terms except the last two include bond-order dependence and depend on the local environment of each atom. The Coulomb energy ($E_{coulomb}$) of the system is calculated using a geometry dependent charge distribution determined using the electro negativity equalization method (EEM [55]). All other non-bonded interactions (short-range Pauli repulsion and long-range dispersion) are included in the van der Waals term ($E_{vdWaals}$). The non-bonded interactions ($E_{coulomb}$ and $E_{vdWaals}$) are screened by a taper function and shielded to avoid excessive repulsion at short distances. For a more detailed description of the ReaxFF method, see van Duin et al.[53] This ReaxFF formalism has been previously employed to simulate the lithiation mechanisms in sulfur [56] and Si NW electrodes [54]. Here, in order to simulate this system, we developed new ReaxFF Li-Si-Al-O parameters in ReaxFF, by adding new training sets of DFT results, such as Li ion diffusion energy barrier, formation and lithiation energy to the existing ReaxFF Li/Si/Al/O description from Narayanan and co-workers [57].

After finishing the development of Li-Si-Al-O parameters of ReaxFF, the reactive MD simulations were performed on amorphous Si core-shell structures, in which the shell was amorphous Al_2O_3 or SiO_2 at different thicknesses. The core-shell structures were surrounded by Li atoms in a 3D periodic simulation boxes at the dimension of 78Å×53Å×72Å. The length of the core shell structure was the same as the length of the y dimension of the simulation box, as shown in Figure 1. This simulates an infinitely long Si nanowire covered by coatings lithiated along the radial directions. More specifically, six simulation sets (listed in table 1) were prepared to investigate coating materials and shell thickness effect upon lithiation to Si nanowire. The initial diameter of Si core is 15Å. The initial thicknesses of shells were 2.5 Å, 4.5 Å and 7.5 Å for SiO_2 and Al_2O_3, respectively. The amorphous Si core consisted of 478 Si atoms with initial density of 2.38 g/cm^3 (compared well with experimental value of 2.33 g/cm^3 .[58]). The densities of initial amorphous SiO_2 and Al_2O_3 were 2.18 g/cm^3 (experimental value of 2.2 g/cm^3 [59, 60]) and 3.16 g/cm^3 (experimental value of 3.1 g/cm^3.[61]), respectively. These amorphous structures were obtained by first melting and quenching, then equilibrating the structures at 298K by NPT ensemble. The initial core-shell structures were constructed based on these equilibrated amorphous structures. Energy minimizations were performed for the core-shell structures surrounded by Li until the energy tolerance of 10^{-5} eV was satisfied or 2000 steps. MD simulations were then carried out in the canonical ensemble (NVT) at the temperature of 900K using the velocity Verlet algorithm with a time step of 0.25 fs. The forces were computed using the ReaxFF, and implemented in the Large-scale Atomic/Molecular Massively Parallel Simulator (LAMMPS) package [62].

The lithiation process of Si-core-oxide-shell structure is spontaneous due to the large negative heat of mixing. Figure 1 shows the cross-section of core-shell structures during the lithiation

process. To facilitate the comparison of the lithiation process in different core-shell structures, the innermost and outermost Si/O (Al/O) atoms in the shell of the initial configurations were tracked during the simulations. Since the atomic shuffling and diffusion in these shell atoms were negligible compared to lithium atoms, the innermost and outmost atoms in the shell stayed mainly as the boundaries of the shell. The average positions of the innermost oxide shell atoms defined the radius of the Si core and those of the outmost oxide shell atoms define the radius of the shell. The Li atoms located outside the core and inside the shell radii were counted as the Li content inside the shell, and those diffused inside the innermost boundary of the shell were counted as the Li in the core and its ratio with Si is the Li content x in the Li_xSi core. When x=3.75, full lithiation of the Si core was reached and the MD simulations were terminated.

3. Results and discussions

3.1 The Chemical and structural evolution of Si core

Figure 2 shows the number of Li atoms in the Si core and the radius of the lithiated Si core with respect to time until full lithiation. As is shown in Figure 2(a), the thin SiO_2 shell (2.5Å) case reaches the fully lithiated state first. The difference between the cases of thin (2.5Å) and intermediate (4.5Å) SiO_2 shells is minor because Li penetrates through very fast (even during minimization stage) in SiO_2 when it is not thick enough. However, for the cases of Al_2O_3, the thickness affects lithiation time significantly since Li moves relatively slowly in Al_2O_3 compared to in SiO_2. [49] The time to reach full lithiaton for the six core-shell structures considered in this study is shown in Table 1. The overall lithiation time and the radii of the core-shell structures follow the relationship of $R_0 \propto \sqrt{t}$. Here we defined an effective diffusion coefficient, D_{eff}, to

describe the lithiation rate as $R_0 = \sqrt{D_{eff}t}$ and obtained it by a linear fitting. The lithiation rate in SiO_2 shell covered Si core is almost four times faster than Al_2O_3 covered Si core.

Figure 2(b) shows the radii of the Si cores and shells with respect to time until the fully lithiated state. The initial Si core radius is only 7.5Å. Due to the periodic boundary condition of the simulation cell, all the volume expansion of the Si core occurs along the radial direction. Therefore, the 300% volume incensement will double the Si core size. Indeed, as shown in Figure 2(b), the final Si core radii of the thin (2.5Å) SiO_2, intermediate (4.5Å) SiO_2 and thin (2.5Å) Al_2O_3 cases are nearly doubled (15Å), which indicates that these shells did not impose significant compressive constraints on the Si core. In comparison, for the thick (7.5Å) SiO_2, intermediate (4.5Å) Al_2O_3, and thick (7.5Å) Al_2O_3 cases, the radii of the Si cores only expands to 14Å, corresponding to a 13 % volume compression compared to the free volume expansion. This is a clear indication of the mechanical constraints imposed by the shell, which also goes through chemical and structural changes.

3.2 The Chemical and structural evolution of the SiO_2 and Al_2O_3 shells

When lithium atoms inserted into the Si-core/SiO_2-shell structures, the SiO_2 shells were immediately lithiated followed by the lithiation of the Si cores. In contrast to the SiO_2 shells, lithiation happened relatively gradually for the Si-core/Al_2O_3-shell models compared to the Si-core/SiO_2-shell models due to the higher Li diffusion energy barrier of Al_2O_3 than that of SiO_2. [49] Figure 3 shows the chemical evolution of the SiO_2 and Al_2O_3 shells until full lithiation of the Si core in terms of Li/Si and Li/Al ratios in the shell. The maximum Li/Si ratio and Li/Al ratio are around 7.0 and 3.5, respectively. This can be explained as follows.

According to DFT calculations [49], the lithiation reactions up to SEI formation voltage (0.8V) can be expressed as

$2Li + SiO_2 \rightarrow 0.5Li_4SiO_4 + 0.5Si$ (2)

As the voltage drops below 0.5V, Li continues to replace the Si out of the Li_4SiO_4, so it gradually becomes Li_2O, and the replaced elemental Si can also be fully lithiated Si ($Li_{15}Si_4$).

$5.75\ Li + 0.5Si + 0.5Li_4SiO_4 \rightarrow 2Li_2O + 0.25(Li_{15}Si_4)$ (3)

Combining reaction (2) and (3) results in

$7.75\ Li + SiO_2 \rightarrow 2Li_2O + 0.25(Li_{15}Si_4)$ (4)

So the theoretical Li/Si ratio can be as high as 7.75. Since the current SiO_2 coated Si exists next to Li metal (at 0V) and the Si core is also fully lithiated (~0.1V), this level of lithiation of the SiO_2 shell is reasonable.

Similarly, for Al_2O_3, the initial lithiation reactions up to SEI formation voltage (0.8V) can be written as

$1.5Li+Al_2O_3 \rightarrow 1.5LiAlO_2 + 0.5Al$ (5)

When the voltage drops below 0.5V, Li atoms continuously replace the Al in the $LiAlO_2$ and gradually form Li_2O, and elemental Al can be lithiated to either LiAl or $Li_{2.25}Al$, according to Li-Al phase diagram. If $Li_{2.25}Al$ is formed, the reaction is

$9Li + 0.5Al + 1.5LiAlO_2 \rightarrow 3Li_2O + 2(Li_{2.25}Al)$ (6)

Combining reaction (5) and (6) yields

$5.25Li+0.5Al_2O_3 \rightarrow 1.5Li_2O + Li_{2.25}Al$ (7)

So, the Li/Al ratio can be as high as 5.25. Based on the current results in Figure 3b, full lithiation of Al did not occur. Instead, the suitable lithiation reaction for the current result is expressed as

$$4Li + 0.5Al_2O_3 \rightarrow 1.5Li_2O + LiAl \quad (8)$$

This is consistent with experimental results on Li-Si composite anode, where $Li_{15}Si_4$ and LiAl were formed at the full lithiation state [63].

The initial, intermediate, and final lithiated amorphous coating materials were calculated using the current force field and tabulated in Table 2 to show the details of the evolving material properties. The lithiation of the coating material causes density decrease, volume expansion, and softening. Table 2 indicates that the Young's modulus for amorphous SiO_2 and lithiated compound of SiO_2 are softer than Al_2O_3 and the lithiated compound of Al_2O_3 at similar Li content. In addition, the volumes of both amorphous Al_2O_3 and SiO_2 increase by 300 % when Al_2O_3 becomes $Li_8Al_2O_3$ and SiO_2 is changed to $Li_{7.75}SiO_2$.

Figure 3 shows that for the thick SiO_2 and Al_2O_3 cases, the Li/Si and Li/Al ratio kept increasing toward, but still remained less than, the theoretical Li/Si and Li/Al ratios up to full lithiation. This is more obvious in the Al_2O_3 case, as the full lithiation ratio may only occur near the outer surface due to the slow diffusion of Li in Al_2O_3. For the 2.5Å and 4.5Å SiO_2 and 2.5Å Al_2O_3 the Li content in the shell increased first and then decreased. This observation is attributed to the fact that these coatings are broken (Figure 4d) so the shell boundaries were not clearly defined as the other cases.

By analyzing the final atomic structures, three coating failure mechanisms are identified. The 2.5Å and 4.5Å SiO_2 shells and 2.5Å Al_2O_3 shell are considered totally broken at the end of the simulations (Figure 4(d)). Therefore, they did not impose any mechanical constraints on the

expanding Si core. We also tracked the position of the Si atoms in the core. After the shell broke, the core Si atoms diffused out of the shell. Thick (7.5Å) SiO_2 and intermediate Al_2O_3 (4.5Å) shells exhibited cracks in the final structures (Figure 4(c)). The cracked coatings still maintained its mechanical integrity and imposed a compressive stress on the Si core. Another indication of the cracked coating is that some of the core Si atoms diffuse to the surface of the shell (Figure 5 (b1)). This is reasonable, as the lithiated Si core is under compression and can be squeezed out of any cracks in the coating. Finally, the thick (7.5Å) Al_2O_3 shell is mechanically intact as shown in (Figure 4(b)) and no core Si atom ever diffused out of the shell (Figure 5 (b2)). More discussions on crack formation in the shell will be given in next section.

As Si expands during lithiation, the coating will be stretched thinner. However, the lithiation of the coating itself also induces volume expansion. To show the details of the geometry change of the coating, Figure 4(a) shows temporal variations of the shell thickness for the six core-shell structures. As shown in Figure 3, the lithiation of the shell is almost instantaneous, proceeding very fast in the first 1ps for SiO_2 and 5ps for Al_2O_3, after which the lithiation rate becomes slower. The lithiation of Si core started after Li penetrated through the shell, as we noticed from the Figure 1. Once started, the lithiation rate is relatively linear with time (Figure 2a), consistent with interface controlled lithiation process in Si. Therefore, the shell thickness is governed by its own volume expansion due to lithiation at the initial stage of time, while the mechanical stretching effect reduces the shell thickness during the later stage of time. This trend is very clear in the two cracked coatings, 7.5Å thick SiO_2 and 4.5Å thick Al_2O_3 shells. For the 7.5Å Al_2O_3 shell, these two competing effects reach dynamic equilibrium and a stable shell thickness of 11Å is obtained after 5 ps, providing a mechanically intact coating. The Li/Si and Li/Al ratios, which are responsible for volume expansion, keep increasing when the shells are thick, and the

stretching effect is more pronounced when the thickness is thin and the lithiated shell is soft. Dramatic coating thickness reduction is observed in the three broken coatings. It should be noted that since we defined the shell thickness based on the initial positions of the shell atoms, after the shells are broken, the boundaries of the shell is no longer well defined. Based on our definition, the shell thickness will be greatly reduced due to smearing of the initial coating boundaries.

3.3 Incorporating lithiation of the coating in coating fracture analysis

Verbrugge et. al. derived an analytical solution for the diffusion induced stress in a core-shell structure [64], and predicted that stress discontinuity occurs at the core-shell interface, which can lead to coating delamination (spalling) or cracking. Based on our MD simulations, neither SiO_2 nor Al_2O_3 coatings showed delamination, but cracks that were initiated at the interface then penetrated through the coating did occur. Since lithiation and volume expansion only occurred along the radial direction of the core-shell structure, the coating was continuously broken into pieces in the radial direction when its thickness is small. These fractures occurred due to a large tensile stress in the coating, as the Si-core is lithiated. For the core-shell structure, our MD simulation results show that when the shell is intact, the core experienced a compression that causes a volume contraction of 13% due to the confinement of the coating, and when shell breaks (for sufficiently thin shells), the core can expand freely up to 300% volume expansion. The lithiation causes a linear lithiation strain of ε_c^* in the core and ε_s^* in the shell. Assuming that the core is under a hydrostatic pressure p due to the confinement of the shell, we can calculate the tensile stresses in the shell as

$$\sigma_s^L = p\frac{R}{2h}, \qquad \sigma_s^A = p\frac{R}{h} \tag{9}$$

where σ_s^L is the tensile stress along the axis, σ_s^A is the stress perpendicular to the axis, h is the thickness of the coating layer, and R is the radius of the Si wire. The chemical potential of the Si core is $\chi = -\Delta G + p\Omega$, where ΔG is the chemical potential for the lithiation reaction between Si and Li, and Ω is the atomic volume of lithium. The critical pressure that stops the lithiation is

$$p = \frac{\Delta G}{\Omega} \tag{10}$$

Combining the above equations results in the maximum attainable stress in the shell as

$$\sigma_s = \frac{\Delta G}{\Omega}\frac{R}{h} \tag{11}$$

As lithiation proceeds, R increases, so σ_s increases. If the coating thickness, h, also increases during lithiation, the degree of σ_s increase due to core expansion will be reduced. This scaling analysis also indicates that the stress in the coating can be controlled by tuning not only the initial thickness of the oxide layer and the radius of the Si wire, but also the growth of both sizes during lithiation. Fracture of the coating occurs in the radial direction when σ_s exceeds the breaking stress of the coating, σ_f^{coat}. Thus, to have a fully mechanically intact coating, the R/h ratio must satisfy, at any given lithiation stage,

$$\frac{R}{h} \le \sigma_f^{coat}\frac{\Omega}{\Delta G} \tag{12}$$

It has been noted in previous studies [65-67] and the results in Table 2, the mechanical properties of Si, coating and the interface are all subject to changes upon lithiation. To estimate the σ_f^{coat} for the SiO_2 and Al_2O_3 coatings, we use their theoretical strength $\sigma_f^{coat} = 0.3E$, where

E is the Young's modulus computed in Table 2 for various lithiated Li-Si-O and Li-Al-O compounds. Therefore, comparing SiO_2 with Al_2O_3 coatings on Si nanowires at the same thickness, Al_2O_3 will tolerate more Si deformation due to larger σ_f^{coat}, consistent with our MD simulations. Other experimental results [24, 25, 40] also have indicated that Al_2O_3 coating on Si electrode is more stable during cycling than uncoated electrode and much fewer cracks were found compared to uncoated (in fact SiO_2 terminated) Si film. Taking the fully lithiated core size and coating, Young's modulus, and assuming $\Delta G \sim 0.5eV$ and $\Omega \sim 9\,cm^3/mol$ [42, 68] will lead to an estimation of the critical coating thickness, which is found to be ~9.2Å for lithiated SiO_2 coating and ~6.0Å for lithiated Al_2O_3 coating. This simple estimation is consistent with our observation that the 7.5Å thick Al_2O_3 becoming 11Å thick stays intact as it is beyond the critical thickness, but the 4.5Å thick Al_2O_3 becoming 7Å thick at full lithiation cannot withstand the Si expansion and showed some cracks and the 2.5 thick Al_2O_3 became fully broken. In terms of SiO_2, none of the fully lithiated coating is beyond the critical thickness, so they either show some cracks or are fully broken.

There are some differences between the SiO_2 and Al_2O_3 coatings, which is not consistent with this simple analytical model. Note that the two SiO_2 shells (2.5Å, 4.5Å) are broken in axial direction, which is consistent with the model, but some part of the thin Al_2O_3 shell (2.5Å) is broken perpendicular to the axial direction. The fact that Al_2O_3 is broken perpendicular to the axis is consistent with the experimental results [24] and indicates that the stress in the core is not hydrostatic. These requires a more detailed investigation on stress and Li distribution in the shells.

3.4 Li concentration gradient induced modulus gradient in the shell protects Si electrode and avoids crack propagation

In order to understand why SiO_2 and Al_2O_3 behave differently even at the same initial thickness, we compared the thick 7.5 Å thick SiO_2 and Al_2O_3 shells in Figure 5. The local average atomic densities as a function of distance to the center of the core-shell structures are plotted at the beginning of the MD simulation after minimization (Figure 5 (a1) and (a2)) and at the moment of having LiSi in the core (Figure 5 (b1) and (b2)). Some interface smearing occurred after the minimization steps before MD, but nevertheless, the boundaries between the Si-core, SiO_2 or Al_2O_3 shells, and the Li outside are clearly separated. When the core is lithiated to LiSi, the boundaries between the lithiated Si-core and the shell is still clear, since both coatings maintained its mechanical integrity. However, two differences can be found. The Si-core atoms diffused to the surface of the SiO_2 coating (25 Å from the center) in Figure (b1), but stopped around ~20 Å from the center (or 6 Å into the coating) in the Al_2O_3 covered Si core-shell structure. This means some cracks have penetrated the SiO_2 coating but not through the Al_2O_3 coating. Another difference is the Li density in the lithiated Al_2O_3 coating showing a slope (indicted by the yellow line). Figure 5 (c1) and (c2) show the cutaway configurations of Si nanowires covered with 7.5Å SiO_2 (c1) and 7.5Å Al_2O_3 (c2) at around LiSi ratio. It clearly indicates that much less Li ions exist in the inner shell of Al_2O_3 forming well-defined lithium concentration gradient along the shell while SiO_2 does not have (Figure 5 (b1) and (b2)). As we observed from the lithiation dynamics, lithiation happens relatively gradually in Al_2O_3 coating, especially as the Li migration energy barrier decreases when Al_2O_3 changes into $LiAlO_2$ [49], making well defined Li density gradient inside the 7.5Å thick Al_2O_3 coating.

The Li concentration gradient causes the mechanical property of the inner shell region to stay stiff and strong and the outer region to become softer [49]. Under elastic deformation, the stronger inside is more resistant to crack nucleation. This inner stiff region is expected to have larger strength and helps to delay crack nucleation. In addition to this, the softer outer layer in the coating releases stress in the coating by forming a stress gradient. Therefore, if there is a crack, the crack will stop propagating. The stress gradient can be best illustrated by the Figure 5 (d1) and (d2) shows the von Mises stress distributions. Note in both the concentration and stress plots, the Si core is only lithiated up to ~LiSi, in order to capture the early stage of stress concentration and potential crack nucleation. In contrast, for the SiO_2 shells, there is no Li density gradient inside the coating (Figure 5 (c1)).and the stress distributes uniformly inside the coating (Figure 5 (d1)). Therefore, crack nucleated at the core/shell interface region will propagate through the shell easily because local stress concentrations occurred in the entire shell. Thus, the harder-inside and softer-outside modulus gradient will cause stress gradient, stop crack propagation, and therefore maintain its mechanical integrity until the full lithiated state. Such gradient coating occurs in many other applications, such as biomaterials. [69-71].

To build up the Li concentration gradient, certain thickness of the coating is required. Figure 6 shows that Li density gradient builds up gradually as the thickness of Al_2O_3 coating increases from 2.5Å to 4.5Å and consequently, lithiated 4.5Å Al_2O_3 shell starts to form stress gradient due to modulus gradient. For the thin Al_2O_3 shell (2.5Å), although it did not have Li density gradient at the fully lithiated state, it has the gradient at the initial stage of the lithiation process. The Li density gradient also causes the elastic modulus gradient as mentioned before. Under this elastic modulus gradient environment, generated stresses are distributed uniformly and the shell can avoid local stress concentration, making it difficult for any crack to propagate along the shell

thickness direction. Instead, created cracks grow along the axial region (delamination) in the innermost circumferential direction. When Li density gradient along the shell disappeared as more lithiation occurs in the shell, this defect region propagates through the shell (Figure 4(d)). This failure mechanism applies to only thin (2.5Å) Al_2O_3. For 4.5Å and 7.5Å Al_2O_3 cases, the Li concentration gradient exists until the fully lithiated state. Contrary to Al_2O_3, generated crack in SiO_2 easily propagate through the coating thickness since it does not have Li density gradient along the shell. Therefore, the optimum coating is 4.5Å Al_2O_3 among the 6 cases considering both Li ion diffusion efficiency and mechanical stability of shell.

The mechanical stability analysis has assumed fully lithiated Si, where the largest volume expansion occurs. Meanwhile, thicker coatings slow down diffusion. Therefore, in theory, the minimum coating thickness that can be mechanically stable is the optimized coating thickness without sacrificing the rate performance of the Si electrodes. More specifically to the concentration gradient in lithiated Al_2O_3 coatings, the thickness of Al_2O_3 coating should be thick enough to hold Li density gradient during lithiation. But, the thicker Al_2O_3, the lower the lithium diffusivity, resulting in longer diffusion time. Therefore, the optimum coating is 4.5Å Al_2O_3 among the 6 cases considering both Li ion charging rate and mechanical stability of shell. In other words, the thresholding coating thickness, which starts to generate Li concentration gradient during lithiation, should be selected for the optimized coating thickness.

4. Conclusions

Molecular dynamics simulations have been conducted to investigate lithiation of Si nanowires covered by SiO_2 and Al_2O_3 shells. As soon as the simulations start, lithiation occurs very fast in

the SiO_2 shell followed by subsequent lithiation to Si core. Due to the large stresses caused by sudden expansion of Si electrode, SiO_2 shells are broken unless the thickness of the SiO_2 shell is comparable to the radius of Si electrode. When lithiation happen to the Si nanowire covered by Al_2O_3 shell, Li ions are inserted relatively gradually into Al_2O_3 shell and Si electrode, making well-defined Li density gradient along the shell. This gradient makes the Young's modulus gradient in the shell during the lithiation and has three positive effects. First, the innermost stiff region of the Al_2O_3 can suppress Si electrode effectively and minimize Si volume expansion. Second, the Al_2O_3 shell gets less stress due to the gradual swelling of Si electrode by giving Li ions slowly to the Si electrode. Last, the Al_2O_3 shell can protect itself by avoiding stress concentration with the help of elastic modulus gradient. Therefore, Al_2O_3 shell is hardly broken compared to SiO_2 shell upon lithiation to Si electrode. When Al_2O_3 was broken for thin case (2.5Å), the crack direction is perpendicular to axial direction, while the SiO_2 is broken in axial direction. This different crack direction is also related to the local stress concentration in the shells. Based on the simulation results of Al_2O_3 coated Si, we propose a modulus gradient coating, softer outside, stiffer inside, is beneficial to avoid coating cracking.

FIGURES

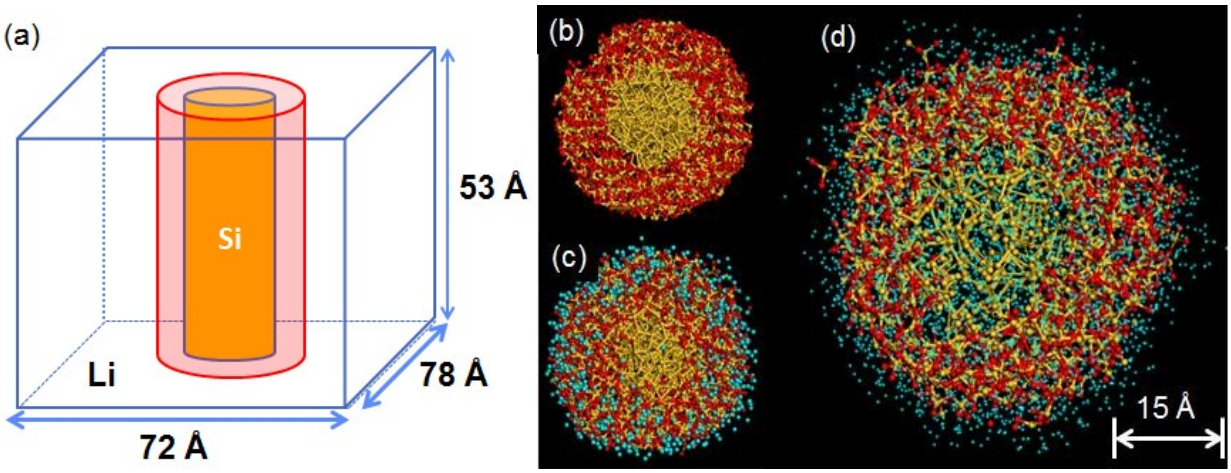

Figure 1. Illustration of the reactive MD simulation of the lithiation process of oxide (shell) covered Si nanowires (core) (Si: yellow, O: red, Li: cyan)

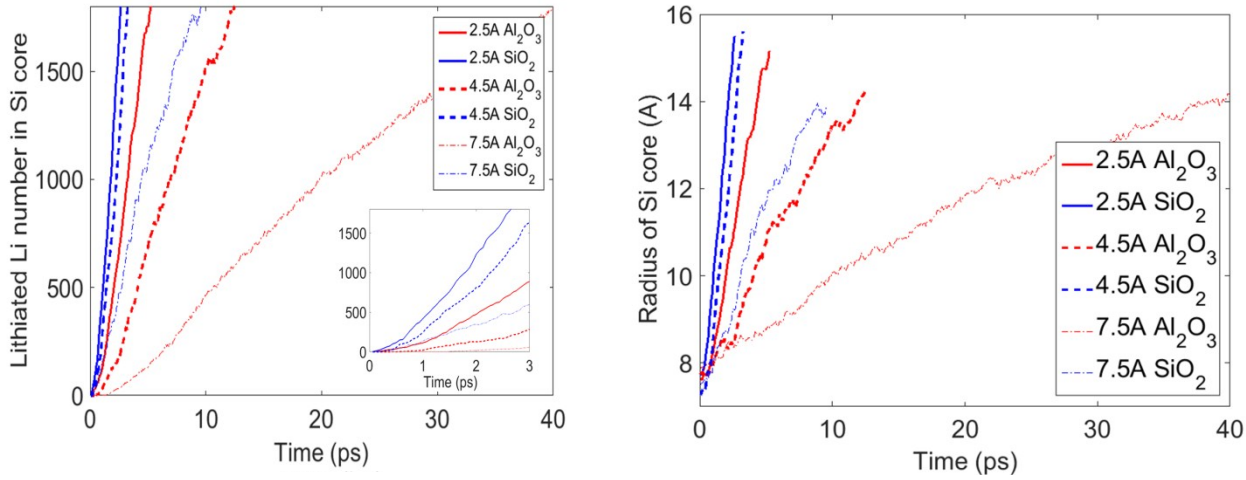

(a) Lithiated Li number in Si core with time (b) Radius of the lithiated Si core with time

Figure 2. The chemical and structural evolution of the Si-core until full lithiation

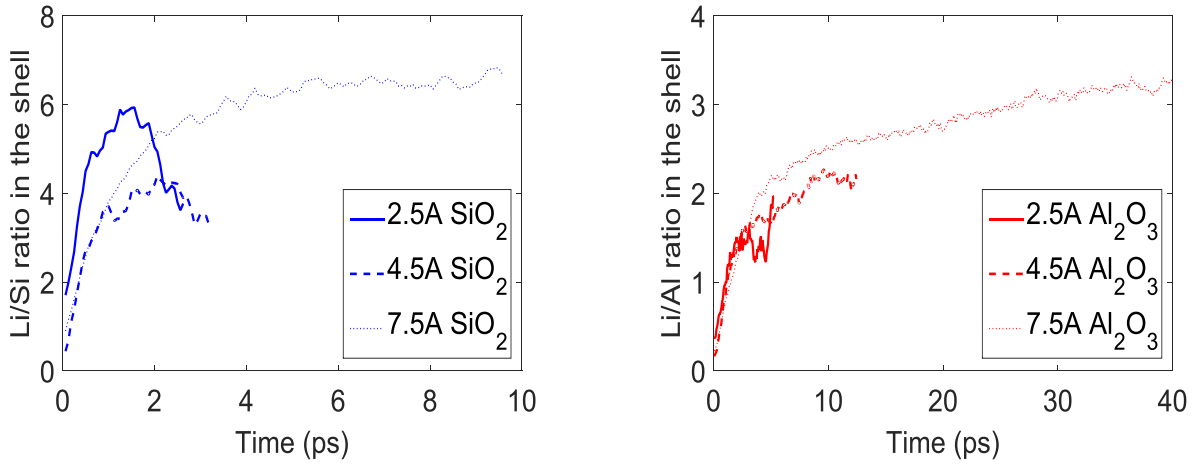

(a) Li/Si ratio in the SiO_2 shell with time (b) Li/Al ratio in the Al_2O_3 shell with time

Figure 3. The chemical evolution of the SiO_2 and Al_2O_3 shells until full lithiation of the Si core.

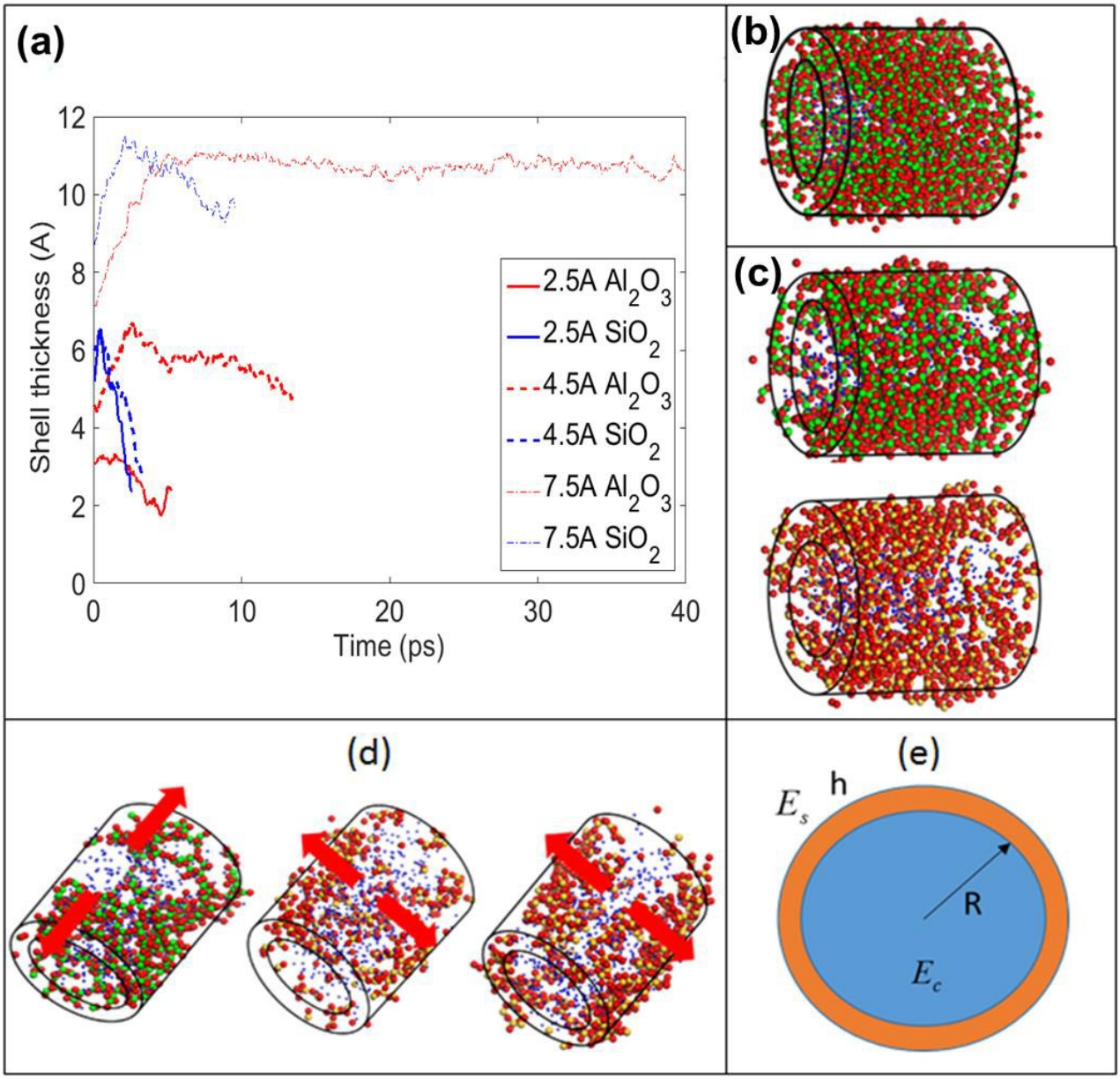

Figure 4. Shell failure mechanisms. (a) Shell thickness with time; (b) mechanically intact shell: 7.5Å Al_2O_3 (c) cracked shell: 4.5Å Al_2O_3, 7.5Å SiO_2 (d) broken shell: 2.5Å Al_2O_3, 2.5Å SiO_2, and 4.5Å SiO_2 (Si(core): blue dot, Si(shell sphere): yellow sphere, O: red sphere, Al: green), and (e) illustration of the core-shell mechanics model.

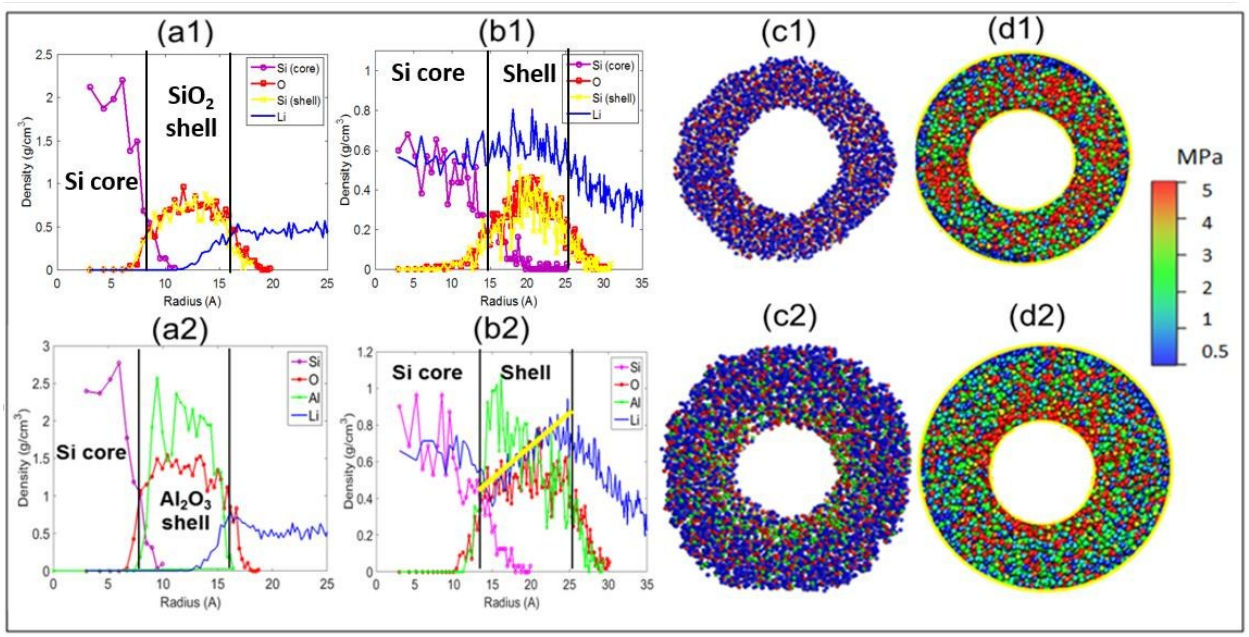

Figure 5. Elemental mapping in the core-shell structure upon lithiation. Densities of elements with radial distance from the center of the Si core at 0.0625 ps for 7.5Å SiO_2 and 7.5Å Al_2O_3. (a1, a2) Densities of elements with radial distance from the center of the Si core when the core is lithiated to LiSi for 7.5Å SiO_2 and 7.5Å Al_2O_3. (b1, b2) Uniformly distributed Li along the SiO_2 shell and gradient Li distribution along the Al_2O_3 shell during lithiation. (c1, c2) von Mises stress distributions for 7.5Å SiO_2 and 7.5Å Al_2O_3 during lithiation showing lower uniformly distributed stresses in Al_2O_3 compared to SiO_2 (d1, d2)

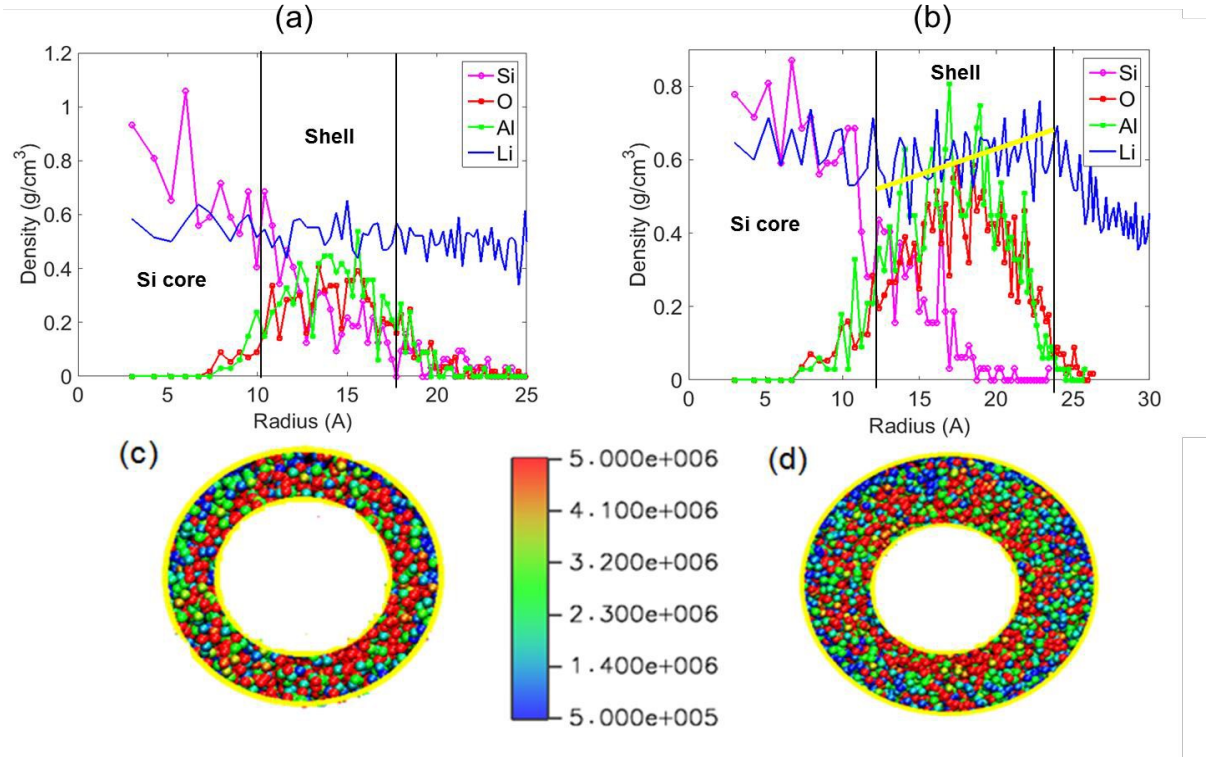

Figure 6. Li density gradient builds up as the thickness of Al_2O_3 coating increases. (a) Densities of elements with radial distance from the center of the Si core at 5.25 ps (fully lithiated) for 2.5Å Al_2O_3, (b) densities of elements with radial distance from the center of the Si core at 12.4 ps (fully lithiated) for 4.5Å Al_2O_3, (c) local stress concentration in the entire coating at 5.25 ps (fully lithiated) for 2.5Å Al_2O_3, (d) starting to avoid local stress concentration as the Li density gradient build up at 12.4 ps (fully lithiated) for 4.5Å Al_2O_3

Table1. The initial shell thickness, and the initial core-shell structure radius, R_0, MD simulation to reach full lithiation of the Si-core, *t*, and the effective diffusion coefficient to lithiate the core-shell structure. D_{eff} is obtained by fitting $R_0 = \sqrt{D_{eff}t}$.

	Initial shell thickness (Å)	R_0 (Å)	Times to reach full lithiation *t* (ps)	D_{eff} (cm^2/s)
Al_2O_3	2.5	10	5.25	3.4×10^{-4}
	4.5	12	12.44	
	7.5	15	39.94	
SiO_2	2.5	10	2.63	15.9×10^{-4}
	4.5	12	3.25	
	7.5	15	9.56	

Table 2. Predicted Young's modulus (Gpa) and density (g/cm^3) for amorphous SiO_2 and Al_2O_3 as well as the corresponding lithiated compounds. The experimental measured data are also listed for comparison.

Li-Al-O	Composition change	a-Al_2O_3	a-$LiAlO_2$	a-$Li_8Al_2O_3$
	Density (g/cm^3)	3.16 (expt.[61]=3.1)	2.55	1.62
	Young's modulus (Gpa)	112.23(expt.[61]=122±12)	88.68	45.56
Li-Si-O	Composition change	a-SiO_2	a-Li_4SiO_4	a-$Li_{7.75}SiO_2$
	Density (g/cm^3)	2.18 (expt.[59, 60]= 2.2)	2.07	1.36
	Young's modulus (Gpa)	70.15(expt.[59,60]= 76.6±7.2)	60.77	28.91

Acknowledgments

SK, YQ, HG, and XX acknowledge the department of energy and the assistant secretary for energy efficiency and renewable energy, (Office of vehicle technologies of the U.S. department of energy under contract No. DE-AC02-05CH11231, Subcontract No-7056410) under the Batteries for Advanced Transportation Technologies (BATT) program. SK and YQ also acknowledges support for developing the model as part of the Nanostructures for Electrical Energy Storage (NEES), an Energy Frontier Research Center funded by the U.S. Department of Energy, Office of Science, Basic Energy Sciences under Award number DESC0001160. ACTvD and AO acknowledge funding from a grant from the U.S. Army Research Laboratory through the Collaborative Research Alliance (CRA) for Multi Scale Multidisciplinary Modeling of Electronic Materials (MSME).

References

1 R. A. Sharma and R. N. Seefurth, *J. Electrochem. Soc.* 1976, **123**, 1763.

2 M. H. Park, M. G. Kim, J. Joo, K. Kim, J. Kim, S. Ahn, Y. Cui and J. Cho, *Nano Lett.* 2009, **9**, 3844.

3 C. K. Chan, H. L. Peng, G. Liu, K. McIlwrath, X. F. Zhang, R. A. Huggins and Y. Cui, *Nat. Nanotechnol.* 2008, **3**, 31.

4 T. D. Hatchard and J. R. Dahn, *J. Electrochem. Soc.*, 2004, **151**,A838.

5 L. Y. Beaulieu, K. W. Eberman, R. L. Turner, L. J. Krause and J. R. Dahn, *Electrochem. Solid State Lett.* ,2001, **4**, A137.

6 L. Y. Beaulieu, T. D. Hatchard, A. Bonakdarpour, M. D. Fleischauer and J. R. Dahn, *J. Electrochem. Soc.*, 2003, **150**, A1457.

7 M. T. McDowell, S. W. Lee, I. Ryu, H. Wu, W. D. Nix, J. W. Choi and Y. Cui, *Nano Lett.* ,2011, **11**, 4018.

8 A. Kohandehghan, P. Kalisvaart, K. Cui, M. Kupsta, E. Memarzadeh and D. Mitlin, *J. Mater. Chem.* ,2013, ***A*** **1**,12850.

9 E. M. Lotfabad, P. Kalisvaart, K. Cui, A. Kohandehghan, M. Kupsta, B. Olsen and D. Mitlin, *Phys. Chem. Chem. Phys.* ,2013, **15**, 13646.

10 R. A. Huggins and W. D. Nix, *Ionics* 6, 2000, **57**.

11 T. K. Bhandakkar and H. J. Gao, *Int. J. Solids Struct.* ,2010, **47**, 1424.

12 J. M. M. de la Hoz, K. Leung and P. B. Balbuena, *Acs Applied Materials & Interfaces*, 2013, **5**, 13457.

13 J. H. Cho and S. T. Picraux, *Nano Lett.* ,2014, **14**, 3088.

14 R. Krishnan, T. M. Lu and N. Koratkar, *Nano Lett.* ,2011, **11**, 377.

15 C. K. Chan, R. Ruffo, S. S. Hong and Y. Cui, *Journal of Power Sources* ,2009, **189**, 1132.

16 X. R. Liu, X. Deng, R. R. Liu, H. J. Yan, Y. G. Guo, D. Wang and L. J. Wan, *ACS Appl. Mater. Interfaces* ,2014, **6**, 20317.

17 X. H. Liu, L. Q. Zhang, L. Zhong, Y. Liu, H. Zheng, J. W. Wang, J. H. Cho, S. A. Dayeh, S. T. Picraux, J. P. Sullivan, S. X. Mao, Z. Z. Ye and J. Y. Huang, *Nano Lett.* ,2011, **11**, 2251.

18 T. D. Bogart, D. Oka, X. T. Lu, M. Gu, C. M. Wang and B. A. Korgel, *ACS Nano,* 2014, **8**, 915.

19 L. Q. Zhang, X. H. Liu, Y. Liu, S. Huang, T. Zhu, L. J. Gui, S. X. Mao, Z. Z. Ye, C. M. Wang, J. P. Sullivan and J. Y. Huang, *ACS Nano* ,2011, **5**, 4800.

20 M. T. McDowell, S. W. Lee, C. M. Wang and Y. Cui, *Nano Energy* , 2012, **1**, 401.

21 E. L. Memarzadeh, W. P. Kalisvaart, A. Kohandehghan, B. Zahiri, C. M. B. Holt and D. Mitlin, *J. Mater. Chem.,* 2012, **22**, 6655.

22 Y. He, X. Q. Yu, Y. H. Wang, H. Li and X. J. Huang, *Adv. Mater.*, 2011, **23**, 4938.

23 J. C. Li, X. C. Xiao, Y. T. Cheng and M. W. Verbrugge, *J. Phys. Chem. Lett.* ,2013, **4**, 3387.

24 H. T. Nguyen, M. R. Zamfir, L. D. Duong, Y. H. Lee, P. Bondavalli and D. Pribat, *J. Mater. Chem.,* 2012, **22**, 24618.

25 Y. Liu, N. S. Hudak, D. L. Huber, S. J. Limmer, J. P. Sullivan and J. Y. Huang, *Nano Lett.* ,2011, **11**, 4188.

26 E. M. Lotfabad, P. Kalisvaart, A. Kohandehghan, K. Cui, M. Kupsta, B. Farbod and D. Mitlin, *J. Mater. Chem.* ,2014, ***A*** **2**, 2504.

27 L. W. Su, Z. Zhou and M. M. Ren, *Chem. Commun.* ,2010, **46**, 2590.

28 K. Leung, Y. Qi, K. R. Zavadil, Y. S. Jung, A. C. Dillon, A. S. Cavanagh, S. H. Lee and S. M. George, *J. Am. Chem. Soc.* ,2011, **133**,14741.

29 W. A. van Schalkwijk and B. Scrosati, *Kluwer, New York*, 2002.

30 K. Xu, *Chem. Rev.* ,2004, **104**, 4303.

31 Y. Wang and P. B. Balbuena, *Imperial College, London,* 2004.

32 Y. S. Jung, A. S. Cavanagh, L. A. Riley, S. H. Kang, A. C. Dillon, M. D. Groner, S. M. George and S. H. Lee, *Adv. Mater.,* 2010, **22**, 2172.

33 P. Katiyar, C. Jin and R. J. Narayan, *Acta Mater.*, 2005, **53**, 2617.

34 R. Deshpande, Y. Qi and Y.-T. Cheng, *J. Electrochem. Soc.,* 2010, **157**, A967.

35 G. Sikha, S. De and J. Gordon, *J. Power Sources* , 2014, **262**,514.

36 S. De, J. Gordon and G. Sikha, *J. Power Sources,* 2014, **262**, 524.

37 G. Sandu, L. Brassart, J. F. Gohy, T. Pardoen, S. Melinte and A. Vlad, *ACS Nano,* 2014, **8**, 9427.

38 X. H. Liu, H. Zheng, L. Zhong, S. Huan, K. Karki, L. Q. Zhang, Y. Liu, A. Kushima, W. T. Liang, J. W. Wang, J. H. Cho, E. Epstein, S. A. Dayeh, S. T. Picraux, T. Zhu, J. Li, J. P. Sullivan, J. Cumings, C. S. Wang, S. X. Mao, Z. Z. Ye, S. L. Zhang and J. Y. Huang, *Nano Lett.* ,2011, **11**, 3312.

39 B. C. Yu, Y. Hwa, C. M. Park, J. H. Kim and H. J. Sohn, *RSC Adv.,* 2013, **3**, 9408.

40 X. C. Xiao, P. Lu and D. Ahn, *Adv. Mater.* ,2011, **23**, 3911.

41 S. Sim, P. Oh, S. Park and J. Cho, *Advanced Materials* , 2013, **25**, 4498.

42 B. W. Sheldon, S. K. Soni, X. C. Xiao and Y. Qi, *Electrochem. Solid State Lett.,* 2012, **15**, A9.

43 V. A. Sethuraman, M. J. Chon, M. Shimshak, V. Srinivasan and P. R. Guduru, *J. Power Sources,* 2010, **195**, 5062.

44 B. Philippe, R. Dedryvere, M. Gorgoi, H. Rensmo, D. Gonbeau and K. Edstrom, *J. Am. Chem. Soc.* ,2013, **135**, 9829.

45 R. A. Huggins, *Electrochim. Acta* , 1977, **22**, 773.

46 M. Maeda, T. Watanabe, Y. Imai, Y. Ishikawa and M. Tabe, *Appl. Surf. Sci.* ,2005, **244**, 61.

47 C. M. Ban, B. B. Kappes, Q. Xu, C. Engtrakul, C. V. Ciobanu, A. C. Dillon and Y. F. Zhao, *Appl. Phys. Lett.* ,2012, **100**,4.

48 Q. Y. Wang, J. Liu, A. V. Murugan and A. Manthiram, *J. Mater. Chem.* ,2009, **19**, 4965.

49 S. Y. Kim and Y. Qi, *J. Electrochem. Soc.*, 2014, **161**, F3137.

50 S. Q. Hao and C. Wolverton, *J. Phys. Chem. C* ,2013, **117**,8009.

51 S. C. Jung and Y. K. Han, *J. Phys. Chem. Lett.* ,2013, **4**, 2681.

52 U. Khalilov, G. Pourtois, A. Bogaerts, A. C. T. van Duin and E. C. Neyts, *Nanoscale* , 2013, **5**, 719.

53 A. C. T. van Duin, S. Dasgupta, F. Lorant and W. A. Goddard, *J. Phys. Chem. A,* ,2001, **105**, 9396.

54 A. Ostadhossein, E. D. Cubuk, G. A. Tritsaris, E. Kaxiras, S. Zhang and A. C. T. van Duin, *Phys. Chem. Chem. Phys.,* 2015, **17**, 3832.

55 W. J. Mortier, S. K. Ghosh and S. Shankar, *J. Am. Chem. Soc.* ,1986, **108**,4315.

56 M. M. Islam, A. Ostadhossein, O. Borodin, A. T. Yeates, W. W. Tipton, R. G. Hennig, N. Kumar and A. C. T. van Duin, *Phys. Chem. Chem. Phys.* ,2015, **17**,3383.

57 B. Narayanan, A. C. T. van Duin, B. B. Kappes, I. E. Reimanis and C. V. Ciobanu, *Modell. Simul. Mater. Sci. Eng.* 2012, **20**.

58 G. E. McGuire, *Semiconductor Materials and Process Technology Handbook* ,1988.

59 H. Ni, X. D. Li and H. S. Gao, *Appl. Phys. Lett.* 2006, **88**.

60 I. Idris and O. Sugiura, *Jpn. J. Appl. Phys. Part 1 - Regul. Pap. Short Notes Rev. Pap.* ,1998, **37**, 6562.

61 G. Alcala, P. Skeldon, G. E. Thompson, A. B. Mann, H. Habazaki and K. Shimizu, *Nanotechnology* , 2002, **13**, 451.

62 Aktulga, Fogarty, Pandit and Grama, *Parallel Computing*, 2012, **38**, 245.

63 I. A. Courtney, J. S. Tse, O. Mao, J. Hafner and J. R. Dahn, *Phys. Rev. B*,1998, **58**,15583.

64 R. C. e. Alkire, P. N. e. Bartlett and J. e. Lipkowski, *Electrochemical engineering across scales : from molecules to processes*, John Wiley & Sons ,2015.

65 V. SHENOY, P. JOHARI and Y. QI, *J. Power Sources* ,2010, **195**, 6825.

66 M. E. Stournara, X. Xiao, Y. Qi, P. Johari, P. Lu, B. W. Sheldon, H. Gao and V. B. Shenoy, *Nano Lett.* ,2013, **13**, 4759.

67 M. E. Stournara, Y. Qi and V. B. Shenoy, *Nano Lett.* ,2014, **14**, 2140.

68 M. N. Obrovac, L. Christensen, D. B. Le and J. R. Dahnb, *J. Electrochem. Soc.*, 2007, **154**, A849.

69 R. Z. Wang and S. Weiner, *Journal of Biomechanics,* 1998, **31**, 135.

70 M.-C. G. Klein and S. N. Gorb, *Journal of the Royal Society Interface* , 2012, **9**, 3140.

71 G. J. Ehlert and H. A. Sodano, *ACS Appl. Mater. Interfaces* ,2009, **1**, 1827.